

Adversarial Robustness Against Image Color Transformation within Parametric Filter Space

Zhengyu Zhao, Zhuoran Liu, and Martha Larson

Abstract—We propose Adversarial Color Enhancement (ACE), a novel approach to generating non-suspicious adversarial images by optimizing a color transformation within a parametric filter space. The filter we use approximates human-understandable color curve adjustment, constraining ACE with a single, continuous function. This property gives rise to a principled adversarial action space explicitly controlled by filter parameters. Existing color transformation attacks are not guided by a parametric space, and, consequently, additional pixel-related constraints such as regularization and sampling are necessary. These constraints make methodical analysis difficult. In this paper, we carry out a systematic robustness analysis of ACE from both the attack and defense perspectives by varying the bound of the color filter parameters. We investigate a general formulation of ACE and also a variant targeting particularly appealing color styles, as achieved with popular image filters. From the attack perspective, we provide extensive experiments on the vulnerability of image classifiers, but also explore the vulnerability of segmentation and aesthetic quality assessment algorithms, in both the white-box and black-box scenarios. From the defense perspective, more experiments provide insight into the stability of ACE against input transformation-based defenses and show the potential of adversarial training for improving model robustness against ACE.

Index Terms—Non-suspicious adversarial examples, principled parametric filter space, attacks and defenses, image enhancement.



1 INTRODUCTION

DESPITE the exceptional success of Deep Neural Networks (DNNs), recent research has shown that they are remarkably vulnerable to *adversarial examples* [1], which are specifically crafted inputs that cause incorrect model predictions. In computer vision, adversarial examples have been extensively studied in basic image classification tasks [2], [3], [4], [5], and have also been explored for other problems, such as object detection [6], [7], semantic segmentation [6], [8], and retrieval [9], [10].

An approach to generating adversarial images is successful if it introduces modifications that escape human notice. Conventional studies have been focused on *indistinguishable adversarial images*, which means that it is difficult to visually distinguish the original and the adversarial image. They generate small perturbations and measure indistinguishability mainly in terms of L_p distance [1], [2], [3], [5], [11], [12], [13], [14], [15], but they also explore more visual-perception-aligned measurements [16], [17], [18], [19], [20], [21], [22]. However, recently, it has been pointed out [23] that when small, indistinguishable perturbations were originally introduced by [1], they were intended only to be an abstract, toy example to facilitate evaluation. In fact, realistic scenarios do not involve direct comparison between the original and the adversarial image. Without direct comparison, image perturbations that do not arouse suspicion can escape notice, and indistinguishability is no longer an important requirement. For this reason, researchers have started to

explore *non-suspicious adversarial images* that accommodate larger perturbations that are not easily noticed because they transform groups of pixels along dimensions consistent with human interpretation of images. Three types of such transformations have been studied in the literature: geometric transformation [24], [25], semantic manipulation [26], [27], [28], and color transformation [29], [30], [31], [32].

Color transformation maintains uniformity at either a local or global level, meaning that similar colors or colors in a particular region are modified in similar ways. Adversarial images created using color transformations are less evident to the human eye and it is possible to add large perturbations without arousing suspicions.

In this paper, we propose Adversarial Color Enhancement (ACE), a novel color transformation approach to generating non-suspicious adversarial images. ACE creates adversarial images by adopting a human-understandable parametric filter, originally developed for image enhancement [33], that approximates common color curve adjustment. The filter is formulated as a single, continuous function, which means ACE is optimized within a principled adversarial action space, and can be systematically controlled by varying the bound on the filter parameters.

The novelty of ACE lies in its principled space, which sets it apart from existing color transformation approaches to creating non-suspicious adversarial images. The state of the art is represented by two approaches that are also optimized with gradient information. First, ReColorAdv [31], which perturbs groups of color-related pixels based on a mapping function with additional constraints on both the local color uniformity and total changes. Second, cAdv [29], which leverages a pre-trained colorization model. The color transformations used by these approaches fail to be continuous, and as a result their action spaces are not well defined, and we do not consider them to be principled. Because

- Z. Zhao and Z. Liu are with the Institute for Computing and Information Sciences, Radboud University, Nijmegen, The Netherlands (e-mail:z.zhao@cs.ru.nl; z.liu@cs.ru.nl).
- M. Larson is with the Institute for Computing and Information Sciences, and the Department of Language and Communication, Radboud University, Nijmegen, The Netherlands, and is also affiliated with the Department of Intelligent Systems, Delft University of Technology (TU Delft), Delft, The Netherlands (e-mail:m.larson@cs.ru.nl).

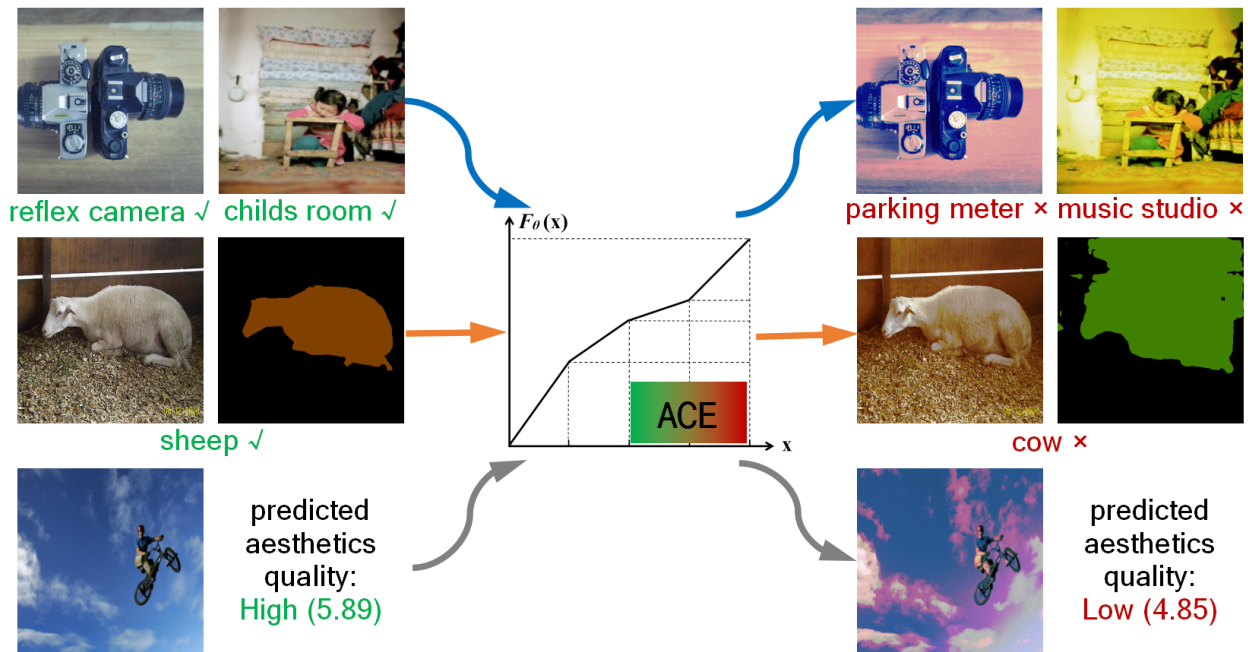


Fig. 1: Overview of our proposed Adversarial Color Enhancement (ACE), which generates adversarial images for different computer vision tasks. From top to bottom: object/scene classification, semantic segmentation, and aesthetic quality assessment. Additional image examples can be found in the GitHub repository.

they are not guided by a principled space, they require techniques such as regularization and sampling to keep the color transformation under control. These techniques obscure the effect of the color transformation, making systematic analysis difficult. In contrast, our ACE operates directly on the parameters of the color filter, which means no additional techniques are necessary. Because ACE can be controlled in a transparent manner, it lends itself naturally to systematic analysis.

In this paper, we introduce ACE and carry out a systematic robustness analysis from both the attack and the defense perspective. We focus on analyzing the vulnerability of image classifiers, but also explore the vulnerability of segmentation and aesthetic quality assessment algorithms, as illustrated in the overview in Fig. 1. In sum, our work makes the following contributions:

- We propose Adversarial Color Enhancement (ACE), a novel approach that generates non-suspicious adversarial images by gradient-based optimization within a parametric color filter space. We investigate a general formulation of ACE and also a variant targeting particular appealing color styles.
- From the attack perspective, we conduct extensive experiments on the vulnerability of image classifiers to ACE in both the white-box and black-box scenarios, but also explore other tasks: semantic segmentation and another previously unexplored but relevant task, aesthetic quality assessment.
- From the defense perspective, we demonstrate the stability of ACE against input transformation-based defenses, and also explore the potential of improving model robustness against ACE based on adversarial training techniques.

This paper substantially extends a preliminary conference version [34] by 1) re-formulating ACE to be directly controlled with bounded filter parameters, facilitating our systematic robustness evaluation, 2) additionally analyzing the problem from the defense perspective, and 3) conducting extensive experiments beyond basic image classification tasks, as shown in Fig. 1. Code is made publicly available at https://github.com/ZhengyuZhao/ACE/tree/master/Journal_version.

2 RELATED WORK

In this section, we cover the most important previous work. For precision, we first provide a formal definition of the creation of adversarial images. A neural network can be denoted as a function $\mathcal{F}(x) = l$ that takes an image $x \in \mathbb{R}^n$ as input and predicts a label l for it. An attack aims to induce a misclassification through modifying the original image x into x' . Accordingly, the attack is regarded as successful should x' be assigned any new class label other than the original one, i.e., $\mathcal{F}(x') \neq l$.

In the remainder of the section, we review related work on conventional small, indistinguishable adversarial perturbations (Sec. 2.1) and also recent studies on non-suspicious adversarial images targeting large perturbations (Sec. 2.2). Finally, we discuss existing defense methods (Sec. 2.3).

2.1 Indistinguishable Adversarial Attacks

Conventional adversarial attacks are focused on small, indistinguishable perturbations, i.e., the adversarial image is restricted to be visually similar to the original image with respect to certain measurements. As already mentioned in Section 1, related work has mainly adopted L_p distance

(L_∞ [2], [3], [11], [12], L_2 [1], [2], [13], L_1 [14] and L_0 [5], [15]), but also explored other measurements that are better aligned with human visual perception [16], [17], [18], [19], [20], [21], [22].

The earliest work [1] on generating indistinguishable adversarial perturbations against the neural networks optimized the joint objective of the misclassification and the L_2 image distance. **C&W** [2] followed a similar formulation, but replaced the cross-entropy loss with a logit-based loss function. Additionally, a new variable was introduced to eliminate the box constraint. This can be expressed as:

$$\min_w \|\mathbf{x}' - \mathbf{x}\|_2^2 + \lambda L_{CW}(\mathbf{x}', l), \quad (1)$$

where

$$\begin{aligned} L_{CW}(\mathbf{x}') &= \max(Z(\mathbf{x}')_l - \max\{Z(\mathbf{x}')_i : i \neq l\}, -\kappa), \\ \text{and } \mathbf{x}' &= \frac{1}{2}(\tanh(\arctanh(\mathbf{x}) + \mathbf{w}) + 1). \end{aligned} \quad (2)$$

Here, L_{CW} is the new loss, \mathbf{w} is the new variable, and $Z(\mathbf{x}')_i$ is the logit with respect to the i -th class given the intermediate modified image \mathbf{x}' . The confidence level of the misclassification can be varied by adjusting κ .

Since such joint optimization suffers from high computational cost due to the need for line search to optimize λ , other methods [3], [11], [12], [13] instead rely on Projected Gradient Descent (PGD) to restrict the perturbations within a small pre-defined L_p norm bound, ϵ . Specifically, the Fast Gradient Sign Method (**FGSM**) [3] was designed to succeed with a single step and has been extended to an iterative variant, **I-FGSM** [11], [12], by exploiting finer gradient information. This can be formulated as:

$$\mathbf{x}'_0 = \mathbf{x}, \quad \mathbf{x}'_{t+1} = \mathbf{x}'_t + \alpha \cdot \text{sign}(\nabla_{\mathbf{x}} J(\mathbf{x}'_t, l)), \quad (3)$$

where α is the step size in each iteration, and \mathbf{x}'_t is the intermediate image obtained at the t -th iteration. In this case, the perturbations larger than a pre-defined L_∞ distance will be clipped. This formulation can also be applied to the L_2 distance by replacing the sign operation with a normalization as $\frac{\nabla_{\mathbf{x}} J(\mathbf{x}'_t, l)}{\|\nabla_{\mathbf{x}} J(\mathbf{x}'_t, l)\|_2}$ [13]. L_0 - and L_1 -based sparse pixel perturbations were also explored [5], [14], [15], [16].

Recently, there have been several attempts to address the limitations of the naive L_p norm bounds by using more visual-perception-aligned measurements to address image indistinguishability. To this end, researchers have explored other advanced similarity metrics, such as the Structural SIMilarity (SSIM) [35], Wasserstein distance [18] and perceptual color distance [20]. Other methods [16], [17], [19] integrate the conventional L_p methods with additional texture information, in order to hide perturbations in image regions that have high visual variation. Instead of direct manipulation of pixel values, local pixel displacement has also been leveraged to generate indistinguishable perturbations [21], [22]. These studies partially relax the tight bounds in conventional L_p methods, leading to a better trade-off between adversarial strength and indistinguishability.

2.2 Non-Suspicious Adversarial Attacks

As already mentioned in Section 1, given the assumption on indistinguishable perturbations being considered to lack compelling examples in the real world, recent work has

started to explore new types of adversarial images that remain non-suspicious to human but allow larger perturbations. Related studies in this direction exploit human-interpretable image transformations, and can be divided into three categories: geometric transformation, semantic manipulation, and color transformation.

Specifically, geometric transformation approaches [24], [25] rely on image translations/rotations to achieve adversarial effects, given the current CNNs being sensitive to such transformations [36]. In order to avoid arousing suspicion, the transformations are constrained to maintain the original concepts, and also content normality (e.g., the sky should be on the top). Semantic manipulation approaches have been mainly explored in specific domains, such as face recognition [27], [28] and road sign recognition [26], where they manipulate the semantically meaningful attribute(s), such as make ups [27], [28] and graffiti [26].

Early work on color transformation searches for possible adversarial images by randomly adjusting the colors of all pixels without any constraints [30]. Later work, ColorFool [32], adopts a similar idea, but imposes additional semantic-aware constraints in local regions, leading to more visually acceptable images. In contrast, recently, the ReColorAdv [31] and cAdv [29] have been proposed to optimize color transformation based on gradient information, leading to more accurate and efficient search for potential adversarial images.

ReColorAdv defines a functional transformation, f , that is operated in a sampled color space \mathcal{G} , with an additional regularization term L_{smooth} on local color uniformity and pixel-wise L_∞ bound to restrict the maximum color changes. The optimization can be formulated as:

$$\min_f L_{CW}(f(\mathbf{x}), l) + \lambda L_{\text{smooth}}(f), \quad (4)$$

where

$$\begin{aligned} L_{\text{smooth}}(f) &= \sum_{g_j \in \mathcal{G}} \sum_{g_k \in \mathcal{N}(g_j)} \|(f(g_j) - g_j) - (f(g_k) - g_k)\|_2, \\ \text{and } \|\mathbf{x} - f(\mathbf{x})\|_\infty &\leq \epsilon. \end{aligned} \quad (5)$$

The L_{smooth} achieves local color uniformity by constraining the similarity between each point $g_j \in \mathcal{G}$ and its neighbours $g_k \in \mathcal{N}$. Specifically, trilinear interpolation is used to determine the values of the pixels that are not on the sampled color space. The L_∞ bound can be higher than that for indistinguishable perturbations, due to the better maintained local color uniformity.

cAdv adopts a pre-trained deep colorization model from [37], and integrates the attack optimization into the process of automatically colorizing gray-scale images:

$$\min_{M, X_{ab}} J(\mathcal{F}(\mathcal{C}(X_L, X_{ab}, M)), l), \quad (6)$$

where \mathcal{C} is the colorization model, and $X_L \in \mathbb{R}^{H \times W \times 1}$ is the L channel of the image in CIELAB color space. The sparse colored input hints $X_{ab} \in \mathbb{R}^{H \times W \times 2}$, which are taken from the original image, and the binary mask $M \in \mathbb{B}^{H \times W \times 1}$ are optimized to achieve the adversarial effects. The similarity between the colorized image and its original ground truth is constrained to make sure the colorization looks realistic.

Our ACE differs from the above color transformation ap-

proaches in the following aspects. Firstly, ACE relies on optimization with gradient information and so fundamentally differs from those random search-based approaches [30], [32]. Specifically, comparisons in Sec. 4.1.5 demonstrate that ACE performs far better than a random search-based alternative. Compared with ReColorAdv, which relies on additional regularization on local color uniformity, sampling and pixel-wise norm bounds, our ACE uses a single, continuous parametric filter function and directly bounds its parameters. Compared with the cAdv, our ACE enjoys a far simpler and transparent formulation, and needs no pre-training on massive data. Extensive analysis in Sec 4.1.1 demonstrates that our ACE yields better performance in terms of both black-box success rates and image quality.

2.3 Adversarial Defenses

As different adversarial attacks raise increasing concerns, corresponding defenses are also being extensively studied. In the scenario where the attack is not aware of the deployment of the defenses, early work [38], [39], [40] has proposed to use data-driven detection methods, based on the assumption that the adversarial images may be drawn from different distributions from normal images. Other defenses leverage common input transformations [41], [42], [43], [44] to eliminate the adversarial perturbations, which require no need of training and have achieved effective results. However, in the more challenging scenario where the attack can be adapted to the specific defense, the detection and transformation defenses have been shown to be vulnerable [45], [46].

Many recent defenses have claimed strong robustness against white-box attacks, but were finally shown to be completely circumvented by simple adaptive attacks [47]. This leaves adversarial training [12], [48] as the only potentially productive way to guarantee empirical model robustness. Adversarial training involves (re-)training neural networks on adversarial examples, in contrast to using the original data as in standard training. In the context of indistinguishable perturbations, early methods trained on the single-step FGSM attack are shown to be insufficient against iterative attacks [11], [49]. In contrast, adversarial training based on iterative Projected Gradient Descent (PGD) has been demonstrated to guarantee perfect robustness on the simple MNIST dataset, and also achieve promising results on the larger-scale CIFAR-10 [12], [48]. However, implementing PGD-based adversarial training on the complex ImageNet remains challenging due to the huge computational overhead. Therefore, many studies [50], [51], [52], [53], [54], [55] have proposed to improve adversarial training in terms of efficiency. Beyond small, indistinguishable perturbations, adversarial training has also been discussed on non-suspicious adversarial images [24], [31], [56].

In this paper, we compare ACE with other attacks in the scenario where the attack is not aware of the defense using the input transformation-based methods. We also explore adversarial training to improve model robustness against ACE, and discuss the relation between ACE robustness and conventionally-studied L_p robustness.

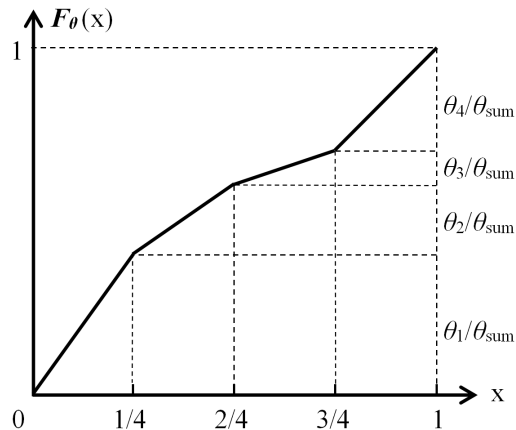


Fig. 2: Illustration of the piecewise-linear color filter in our ACE (with four pieces, i.e., $K = 4$ in Eq. 7).

3 APPROACH

In this section, we first introduce the parametric image color filter on which we build Adversarial Color Enhancement (ACE), our new attack approach for generating non-suspicious adversarial images. Then, we describe the general formulation of ACE, which uses a parameter bound, and also a variant targeting particular appealing color styles.

3.1 Parametric Image Enhancement Filters

The state of the art for automatic photo enhancement mainly uses supervised learning to determine editing parameters, in order to achieve specific image appearances. Most approaches [57], [58], [59] utilize DNNs for parameterization and, consequently, suffer from high computational cost and more importantly, they are not understandable to users. In contrast, recent work [33], [60] has proposed to rely on intuitively meaningful edits that are represented by conventional post-processing operations, i.e. image filters, to make the automatic process human-understandable. Such methods have far fewer parameters to optimize, and can be applied independently of the image resolution.

In this work, we adopt the monotonic piecewise-linear function in [33], which approximates the common color curve adjustment, for our filter, due to its simplicity. This filter can be formulated as:

$$F_{\theta}(x_k) = \sum_{i=1}^{k-1} \frac{\theta_i}{\theta_{\text{sum}}} + (K \cdot x_k - (k-1)) \cdot \frac{\theta_k}{\theta_{\text{sum}}}, \quad (7)$$

$$\theta_{\text{sum}} = \sum_{k=1}^K \theta_k,$$

where K demotes the total number of pieces. In this case, an input image pixel x_k whose value falls into the k -th piece of function will be filtered using the parameter θ_k , and $F_{\theta}(x_k)$ is its corresponding output. By doing this, pixels with similar colors will be filtered with the same parameter, leading to uniform color transformation. Specifically, the three RGB channels are processed independently. An example of this function with four pieces ($K = 4$) is illustrated in Fig. 2.

Algorithm 1 Adversarial Color Enhancement (ACE)-PGD**Input:** x : original image, l : original label, T : number of iterations α : step size, ϵ : bound of parameters F_θ : color filter with parameters θ (K -dimensional)**Output:** x' : adversarial image

```

1: Initialize  $\theta_0 \leftarrow \mathbb{1}^K / K$ ,
2:    $x'_0 \leftarrow F_{\theta_0}(x)$ 
3: for  $t \leftarrow 1$  to  $T$  do
4:
5:    $g \leftarrow \nabla_{\theta} L_{CW}(x'_{t-1}, l)$   $\triangleright$  calculate gradients w.r.t.
                                     the C&W loss
6:    $\theta_t \leftarrow \theta_{t-1} - \alpha \frac{g}{\|g\|_2}$   $\triangleright$  update parameters
7:
8:    $\theta_t \leftarrow \text{clip}(\theta_t, \theta_0, \epsilon \theta_0)$   $\triangleright$  clip parameters into the
                                               bounded range
9:    $x'_t \leftarrow F_{\theta_t}(x)$   $\triangleright$  transform the image with
                                     the updated filter
10: end for
11: return  $x' \leftarrow x'_t$  that is adversarial

```

3.2 Adversarial Color Enhancement

This section introduces our novel Adversarial Color Enhancement (ACE), which generates non-suspicious adversarial images by iteratively optimizing the parameters of the color filter defined in Eq. 7.

Parameter bound. We propose to systematically control the color transformation by directly imposing adjustable bounds on the filter parameters. Note that this bound is not necessarily set to create indistinguishable perturbations, since our color filtering can inherently guarantee the uniformity of the image transformation even when the perturbations are large. We refer to this general formulation ACE-PGD, and its full process is described in Algorithm 1.

Color style guidance. The use of a color filter makes it possible to achieve adversarial strength and image enhancement at the same time, by incorporating additional guidance from common enhancement practices into the adversarial optimization. Here, specifically, we propose to target appealing color styles that are determined by popular Instagram filters, and the optimization can be modified to:

$$\min_{\theta} L_{CW}(F_{\theta}(x), l) + \lambda \cdot \|F_{\theta}(x) - x_{\text{ins}}\|_2^2, \quad (8)$$

where x_{ins} denotes the targeted Instagram filtered image with a specific color style.

We refer to this variant of ACE that targets specific Instagram styles as ACE-Ins. We consider two popular Instagram filter styles, Nashville and Toaster, and automate their implementation using the GIMP toolkit with the Instagram Effects Plugins¹. Note that the style shifts in our ACE-Ins are only for enhancement, but not for adversarial effects. ACE-Ins is thus different from the studies of model performance degradation caused by common style shifts [61], [62].

1. https://www.marcocrippa.it/page/gimp_instagram.php.

4 EXPERIMENTS

In this section, we carry out extensive experiments to systematically analyze the model robustness from both the attack and defense perspectives. If not mentioned specifically, ACE refers to its general formulation, ACE-PGD, with $K = 64$, $\epsilon = 16$, and $T = 100$. ACE-Ins is optimized using Adam [63] with a learning rate of 0.01 and 500 iterations. Early stopping is triggered when the optimization no longer makes progress [2], [13]. All the experiments are conducted on a single NVIDIA Tesla P100 GPU with 12GB of memory.

4.1 Evaluation of Attacks

In this subsection, from the attack perspective, we quantitatively evaluate ACE in terms of both the white-box and black-box success rates. We also discuss the visual appearances of the images generated by ACE. Specifically, we compare ACE with other attacks and conduct hyperparameter analysis on the basic ImageNet object classification (Sec. 4.1.1), and also demonstrate the general effectiveness of ACE in other tasks: scene recognition (Sec. 4.1.2) and semantic segmentation (Sec. 4.1.3). In particular, we explore another task, aesthetic quality assessment (Sec. 4.1.4), which is relevant to our problem but has not been explored so far.

4.1.1 Object Classification

The classification of object images is one of the basic problems in computer vision and has been studied for decades. Adversarial images have also been discussed mainly against object classifiers. Following the common practices, we use the official development set of the ImageNet-Compatible Dataset [64], which was introduced along with the NIPS 2017 Competition on Adversarial Attacks and Defenses. It consists of 1000 color images (with the size of 299×299) associated with 1000 ImageNet class labels. We will compare our ACE with the following five gradient-based attacks:

- **FGSM** [3] (indistinguishable) with $\epsilon = 2/255$.
- **I-FGSM** [11] (indistinguishable) with $\epsilon = 2/255$ and 10 iterations.
- **C&W** [2] (indistinguishable) with L_2 norm constraint, and fewer iterations and higher confidence level (iters= 3×100 and $\kappa = 40$) than usual for stronger adversarial effects.
- **ReColorAdv** [31] (non-suspicious) with original settings, $\epsilon = 16/255$, lr=0.001, and $T = 300$, and another variant, ReColorAdv⁺ with more aggressive settings ($\epsilon = 51/255$ and lr=0.005), for stronger adversarial effects.
- **cAdv** [29] (non-suspicious) with original optimal settings, $k = 8$ and $T = 500$, and another more aggressive variant, cAdv⁺, with $k = 4$. cAdv is limited to 224×224 image size due to the fixed output resolution of its adopted pre-trained deep colorization model.

We consider five diverse classifiers: AlexNet [65], ResNet50 [66], VGG19 [67], DenseNet121 [68], and Inception-V3 [69]. Specifically, Inception-V3 is adopted as the white-box model for comparing different approaches because it is the official model used in the NIPS 2017 Competition as mentioned above.

TABLE 1: Success rates of different attacks in the white-box (Inc3) and black-box scenarios in ImageNet object classification. L_0 is the proportion of the perturbed pixels and L_∞ is shown in $[0,255]$. Values of ϵ and K are indicated as ACE-PDG $_{K}^{\epsilon}$. ACE-Ins1 denotes our color Instagram-guided optimization with Nashville filter style, and ACE-Ins2 is with Toaster. The black-box success rates is calculated on images for which the two models' prediction is the same.

| | L_p Norm | | | Inc3 | Success Rate | | | |
|--------------------------|------------|-------|------------|-------------|--------------------|-------------------|-------------------|--------------------|
| | L_0 (%) | L_2 | L_∞ | | \rightarrow Alex | \rightarrow R50 | \rightarrow V19 | \rightarrow D121 |
| FGSM [3] | 49.34 | 4.05 | 2.00 | 78.1 | 7.84 | 5.40 | 5.74 | 5.50 |
| I-FGSM [11] | 39.23 | 3.09 | 2.00 | 99.1 | 8.16 | 4.95 | 6.44 | 4.71 |
| C&W [2] | 29.06 | 3.00 | 15.66 | 99.6 | 8.16 | 4.72 | 6.79 | 4.38 |
| ReColorAdv [31] | 70.81 | 18.87 | 64.00 | 79.3 | 9.76 | 4.50 | 3.40 | 2.58 |
| ReColorAdv ⁺ | 82.50 | 47.53 | 97.21 | 89.2 | 31.20 | 15.64 | 13.58 | 10.77 |
| cAdv [29] | 41.42 | 20.54 | 116.15 | 91.8 | 30.08 | 11.25 | 11.01 | 13.47 |
| cAdv ⁺ | 82.51 | 20.63 | 114.74 | 99.3 | 46.72 | 26.88 | 27.75 | 28.17 |
| Our ACE-PDG $_{32}^8$ | 96.62 | 69.75 | 77.38 | 80.0 | 51.84 | 26.55 | 26.70 | 24.02 |
| Our ACE-PDG $_{64}^{16}$ | 96.80 | 80.57 | 89.64 | 88.7 | 57.76 | 37.01 | 30.21 | 28.96 |
| Our ACE-Ins1 | 97.22 | 82.23 | 84.15 | 93.2 | 43.84 | 20.81 | 22.37 | 17.06 |
| Our ACE-Ins2 | 96.42 | 68.90 | 80.33 | 93.8 | 49.28 | 21.48 | 21.66 | 17.96 |



Fig. 3: Adversarial images (top) and their perturbations (bottom) by different iterative approaches. From left to right: I-FGSM [11], C&W [2], ReColorAdv⁺ [31], cAdv⁺ [29], and our ACE. ACE and ReColorAdv⁺ yield globally uniform color transformation, but ReColorAdv⁺ causes color fading effects. cAdv⁺ introduces local colorization artifacts in the clouds.

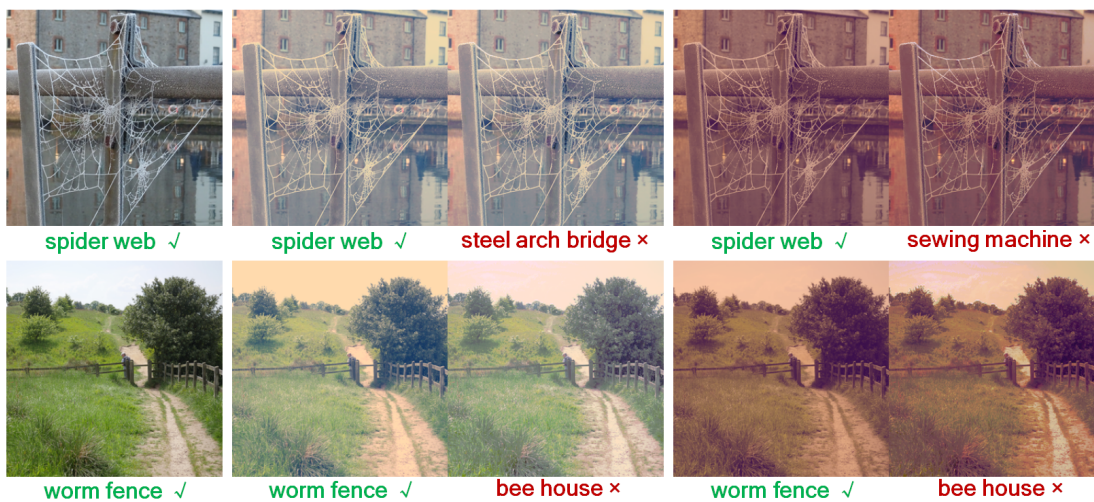


Fig. 4: Images achieved by common Instagram filters and ACE-Ins, which is guided by specific Instagram filter styles. For each pair of images, the left one is processed by a common Instagram filter and the right image is generated by ACE-Ins. The generated adversarial images can achieve both misclassification and specific appealing appearances (correct labels are shown by ✓ and adversarial labels shown by ✗).

TABLE 2: Success rates of ACE (ACE-PGD/-Ins1/-Ins2) in ImageNet object classification. Results are measured with respect to the models in the columns when applying ACE to the models in the rows. Black-box results are off-diagonal.

| | →AlexNet | →ResNet50 | →VGG19 | →DenseNet121 | →Inception-V3 |
|--------------|------------------------|-----------------------|-----------------------|-----------------------|-----------------------|
| AlexNet | 99.5/99.9/100.0 | 37.48/14.65/14.17 | 26.29/13.23/14.52 | 23.25/12.42/14.81 | 15.04/8.64/8.64 |
| ResNet50 | 70.39/46.30/53.70 | 96.8/99.3/99.4 | 34.81/20.14/22.93 | 32.73/19.07/18.74 | 17.21/11.47/9.90 |
| VGG19 | 66.77/45.97/50.97 | 41.33/19.21/19.56 | 95.7/99.0/99.2 | 31.37/15.28/17.48 | 16.04/9.84/12.76 |
| DenseNet121 | 65.76/48.09/51.91 | 44.81/20.32/20.99 | 34.03/21.06/19.56 | 94.9/99.2/98.9 | 16.27/11.56/9.67 |
| Inception-V3 | 57.76/43.84/49.28 | 37.01/20.81/21.48 | 30.21/22.37/21.66 | 28.96/17.06/17.96 | 88.7/93.2/93.8 |

TABLE 3: Success rates of ACE in Places scene recognition.

| | →AN | →R18 | →R50 | →D161 |
|--------------------|-------------|-------------|-------------|-------------|
| AlexNet (AN) | 99.8 | 48.97 | 41.53 | 38.05 |
| ResNet18 (R18) | 77.91 | 98.2 | 53.83 | 47.38 |
| ResNet50 (R50) | 74.49 | 62.43 | 97.2 | 50.47 |
| DenseNet161 (D161) | 74.94 | 56.89 | 58.03 | 94.5 |

As can be seen from Table 1, the L_p approaches I-FGSM and C&W achieve the best white-box results by fully leveraging pixel-level gradients. Color transformation approaches achieve comparable white-box results, while largely outperforming L_p approaches on black-box success rates. As shown in Fig. 3, color transformation approaches yield more visually acceptable image appearances without noise-like perturbations as those in L_p approaches.

Among all the color transformation approaches, our ACE-PGD achieves the best results in the black-box scenario, without sacrificing the color uniformity of the images, as shown in Fig. 3. ReColorAdv⁺ improves on ReColorAdv by allowing more perturbations, indicated by its larger L_p distance. Nevertheless, it causes color fading due to the looser bounds imposed on the luminance channel than the color channels [31]. The cAdv inevitably introduces local colorization artifacts due to the use of sampled hints [29]. The two ACE-Ins variants yields slightly better white-box performance, probably because of the more iterations and the use of Adam optimizer for more accurate gradients, but with lower black-box performance. At the same time, they can achieve specific appealing color styles, as shown in Fig. 4. For comparison we mention that, directly applying the two Instagram filters to the original images decreases the model accuracy by only 13.4% and 12.2%, suggesting that the adversarial strength of our ACE-Ins is not because of the style shifts.

More black-box results in Table 2 further confirm the general effectiveness of ACE for different model architectures. When comparing the results between different architectures, we find that the adversarial effects are generally easier to transfer from a sophisticated architecture (ResNet50, VGG19, DenseNet121, or Inception-V3) to a simple one (AlexNet) than the other way around. Specifically, Inception-V3 is the hardest architecture to attack in both the white-box and black-box scenarios.

4.1.2 Scene Recognition

Recognizing scenes is challenging since it involves understanding the context of the characteristic concepts in different scene categories. We consider a specific task called Pixel

Privacy [70], which was introduced by the MediaEval Multimedia Benchmark, and has been explored in the following work on adversarial images [32], [71], [72]. This task is focused on developing image modification techniques that can protect privacy-sensitive scene information of users against automatic inference of privacy-sensitive scene information.

Our ACE is particularly suitable for this task because the filtered images will be widely acceptable by users since they are generated in a way that is aligned with common practices for photo enhancement. We use the official development set containing 600 images from 60 privacy-sensitive scene categories in the large-scale Places database [73]. We test all the four classifiers (AlexNet, ResNet18, ResNet50, and DenseNet161) that are available in the official PyTorch implementation of the original Places work [73].

Table 3 shows that our ACE can effectively attack the scene recognition models in both the white-box and black-box scenarios. For comparison, we mention that ACE-PGD surpasses recent ColorFool [32], which also explores this task, by 30% (absolute) on the black-box performance, but need fewer iterations (100 vs. 1000). When comparing the results with those in Table 2, we find that scene recognition is generally easier to attack than object classification. This can be explained by the fact close scene categories inherently share similar characteristic concepts, which makes the prediction easier to change [74], [75].

4.1.3 Semantic Segmentation

Semantic segmentation can be regarded as a pixel-level classification process, i.e., linking each pixel in an image to a class label. Existing research on the adversarial vulnerability of semantic segmentation algorithms has been focused on small, indistinguishable [6], [8]. Here we study this problem in the context of color transformation for the first time, by evaluating these algorithms against our ACE.

Specifically, we use the official validation set (1449 images) of the Pascal VOC dataset [76], which consists of internet-images labelled with 21 different object classes, and has been used in the PASCAL Visual Object (VOC) Benchmark. We consider two different state-of-the-art algorithms: Deeplab-v3 [77] and PSPNet [78]. For each of them, we consider two different model architectures: ResNet-50 and ResNet-101. Following [8], we report the mean Intersection over Union (mIoU) Ratio – the ratio of the mIoU on adversarial images to that on original images.

As can be seen from Table 4, our ACE effectively fools all the models in the white-box scenario, and such fooling effects can transfer between different architectures and algorithms. Specifically, in both the white-box and black-box scenarios, the PSPNet is substantially less robust than

TABLE 4: Adversarial performance of ACE in semantic segmentation. The mean IoU Ratio (mIoU-R) is reported (lower means stronger attacks). We consider Deeplab-v3 with ResNet50 (DL-50) and ResNet101 (DL-101) [77], PSP-Net with ResNet50 (PSP-50) and ResNet101 (PSP-101) [78].

| mIoU-R (%) | DL-50 | DL-101 | PSP-50 | PSP-101 |
|------------|--------------|--------------|--------------|--------------|
| DL-50 | 44.77 | 73.82 | 60.94 | 62.41 |
| DL-101 | 76.56 | 44.62 | 64.43 | 65.27 |
| PSP-50 | 74.94 | 74.77 | 27.60 | 47.79 |
| PSP-101 | 73.08 | 70.93 | 44.21 | 31.02 |



Fig. 5: Adversarial images generated by ACE for semantic segmentation. Left: original images with their ground-truth segmentation maps. Right: adversarial images with their segmentation maps predicted by PSPNet-ResNet50. Different colors denote different object classes.

Deeplab-v3 against our ACE, despite its higher accuracy on original images (mIoU 73.94 % vs. 68.64% with ResNet-50). This difference may be because the dilated convolution in Deeplab-v3 can learn features at multiple scales, making it harder for the attacks to find a global solution.

Fig. 5 shows adversarial images generated by our ACE-PGD. Due to the color uniformity of ACE, the predicted segmentation maps generally corrupt along human-interpretable dimensions, and can be categorized into, from top to bottom, hiding the foreground objects (false negative), disturbing the background (false positive), and misclassifying the objects. Such results are essentially different from the irregular corruptions of the segmentation maps in previously studied small, indistinguishable perturbations [8].

4.1.4 Aesthetic Quality Assessment

Aesthetic Quality Assessment (AQA) has become increasingly popular with the prevalence of social multimedia. Nonetheless, to the best of our knowledge, until now, there is no research on evaluating the robustness of AQA algorithms against adversarial examples. We fill this gap by applying ACE to decrease the model predicted aesthetic scores of high-quality images, without sacrificing their actual aesthetics. We use the AVA dataset [79], which consists

TABLE 5: Adversarial performance in aesthetics assessment.

| | Original | I-FGSM | ACE |
|-------|----------|--------|------|
| Score | 6.01 | 3.56 | 4.88 |

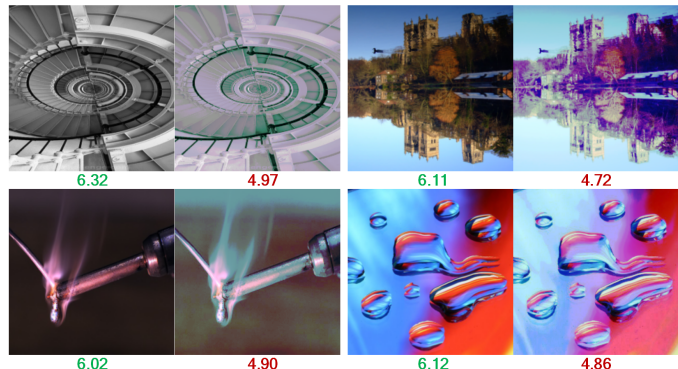


Fig. 6: Adversarial images generated by ACE-PGD against the aesthetic quality assessment model NIMA. Images are shown with their predicted scores.

of over 250000 images along with ratings on their aesthetic qualities by a number of amateur photographers. These ratings range from 1 to 10, with a mean around 5.5. The top 1000 high-quality images from the validation set are selected for our experiments and the averaged results over these images are reported. We consider a well-known AQA model called NIMA (Neural Image Assessment) [80], which learns the distribution of human ratings by training a single CNN (here, VGGNet) with only image-level annotations.

The action space of ACE corresponds more closely to the action space used by photographers when creating photos with high aesthetics. In Fig. 6, it can be seen that ACE can cause the aesthetics score to decrease to below average without a corresponding decrease in aesthetics from the human perspective.

As can be seen from Table 5, our ACE-PGD can effectively decrease the predicted score below 5, which is commonly used as cut off to differentiate images of high and low aesthetic quality [80]. When we guide the images towards specific appealing color styles using ACE-Ins, it becomes slightly harder to fool the model. The results also show that the NIMA model is more robust against ACE than I-FGSM, which exploits finer pixel-level gradient information. This finding is expected and suggests that NIMA has successfully learned robust aesthetic features, which typically lie in the global image styles or subject matter [80].

4.1.5 Hyperparameter Analysis

We analyze the impact of all important hyperparameters of ACE in the basic ImageNet classification. As shown in Fig. 7, in general, the success rates of ACE are gradually increased as we use more iterations, and the performance becomes stable within 100 iterations. We can also observe that increasing the number of pieces, K , leads to better performance by allowing more fine-grained color changes, but at the cost of computational time. In addition, as expected, relaxing the parameter bound, ϵ , boosts the performance by expanding the searching space for possible adversarial examples.

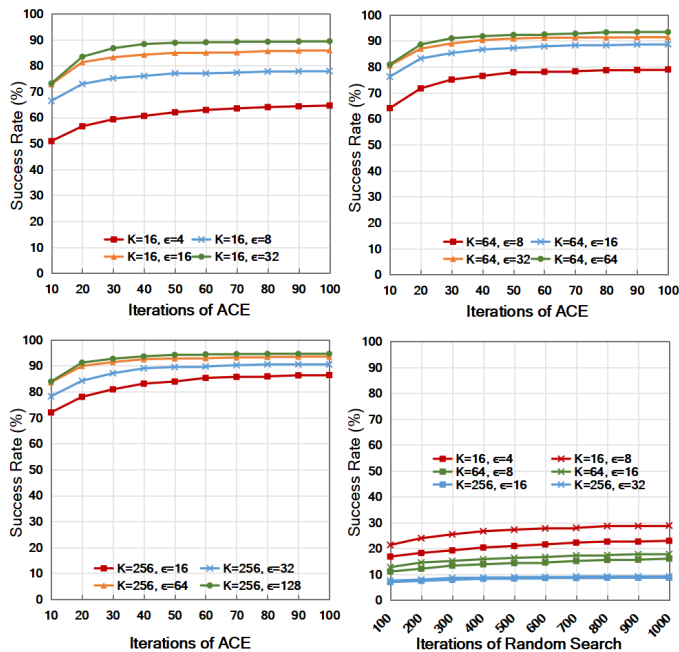


Fig. 7: White-box success rates of ACE and its random search-based alternative with varied K and ϵ , presented as a function of iteration numbers.

As shown by the image examples in Fig. 8, we can observe that as the parameter bound, ϵ , is gradually relaxed, the color changes become increasingly larger. Based on the above findings, in this paper, we choose a moderate $K = 64$ and $\epsilon = 16$ for a good trade-off between the adversarial strength and visual quality.

We also compare our gradient-based ACE with a random search-based alternative that uniformly samples color filter parameters within the searching space defined by a specific K and ϵ . Fig. 7 shows that the adversarial strength of random search is not comparable with our ACE, even when using 10x iterations. Moreover, with a exponentially expanded searching space caused by a higher K , it becomes much harder for random search. In contrast, our ACE can consistently be improved by increasing K , benefiting from its accurate search based on gradients. For comparison we mention that, the random search-based ColorFool [32] has



Fig. 8: Original images and their adversarial versions created by ACE-PGD using $K = 64$ with varied parameter bound, ϵ , from left to right, as 4, 16, and 64.

a success rate of 64.6% (65.4%) with 1000 (1500) iterations when testing on the same experimental settings.

4.2 Evaluation of Defenses

In this subsection, from the defense perspective, we evaluate ACE and other attacks against diverse common input transformations, which have been extensively adopted as the core in many defenses (Sec. 4.2.1). In addition, we explore the potential of adversarial training for improving model robustness against ACE (Sec. 4.2.2).

4.2.1 Input Transformation-based Defenses

Existing work has applied common input transformations as defenses against adversarial attacks without sacrificing the model performance on the original images [41], [42], [43], [44]. We evaluate ACE and other attacks under such defenses by considering a diverse set of transformations:

JPEG compression. We consider two levels of compression with the quality factor as 70 (mild) and 30 (strong).

Scaling. For each 299×299 image, we consider downsampling to 256×256 (mild) and 224×224 (strong), and also upsampling to 384×384 (mild) and 512×512 (strong).

Median smoothing. We consider two different sliding window sizes: 3×3 (mild) and 5×5 (strong).

Grayscale. We expect converting to grayscale to be specifically useful against color transformation attacks.

TABLE 6: Success rates of different gradient-based adversaries against diverse input transformations: JPEG compression, upsampling (U), downsampling (D), median smoothing (MED), and gray-scale conversion (GRAY). The first row reports the results when only the input transformations are applied to the original images without attacks. The downsampling is not applicable to cAdv since its original image size is 224×224 . Inception-V3 is used as the target model.

| | w/o | JPEG70 | JPEG30 | U384 | U512 | D256 | D224 | MED3 | MED5 | GRAY |
|------------------------------|-------|--------|--------|------|------|------|------|------|------|------|
| Original | 100.0 | 5.1 | 9.0 | 8.3 | 11.0 | 12.6 | 19.3 | 15.3 | 28.0 | 14.9 |
| I-FGSM [11] | 99.1 | 61.9 | 25.7 | 39.5 | 22.3 | 42.8 | 32.9 | 52.1 | 39.4 | 83.8 |
| C&W [2] | 99.6 | 54.8 | 23.3 | 40.1 | 23.6 | 36.9 | 29.4 | 42.2 | 35.4 | 89.9 |
| ReColorAdv ⁺ [31] | 89.2 | 33.4 | 27.5 | 24.1 | 22.7 | 38.0 | 39.7 | 43.4 | 50.2 | 22.6 |
| cAdv ⁺ [29] | 99.3 | 80.2 | 62.7 | 34.5 | 35.7 | - | - | 83.2 | 72.5 | 33.1 |
| ACE-PGD | 88.7 | 50.1 | 46.8 | 41.5 | 37.2 | 55.6 | 55.2 | 60.6 | 65.9 | 30.9 |
| ACE-Ins1 | 93.2 | 26.9 | 30.8 | 26.3 | 25.7 | 38.5 | 42.6 | 48.2 | 58.4 | 26.0 |
| ACE-Ins2 | 93.8 | 27.7 | 30.9 | 28.5 | 27.0 | 38.7 | 44.9 | 45.2 | 56.9 | 27.8 |

TABLE 7: Accuracy of different models on original, and adversarial images achieved by PGD and ACE. AT-PGD: model with adversarial training on L_∞ -based PGD, AT-ACE: model with adversarial training on ACE.

| Acc (%) | w/o AT | AT-PGD | AT-ACE |
|----------|--------|--------|--------|
| Original | 95.85 | 86.67 | 87.24 |
| PGD | 7.75 | 49.60 | 5.51 |
| ACE | 7.14 | 16.46 | 54.01 |

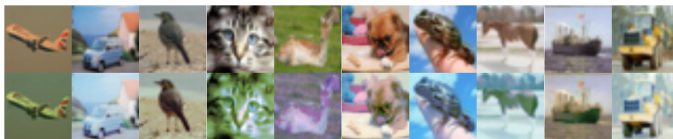


Fig. 9: Image examples (top) and their adversarial versions (bottom) generated by ACE-PGD₆₄⁸ for all the ten classes of images in CIFAR-10.

As shown in Table 6, different attacks are vulnerable to different input transformations. Color transformation approaches are generally stronger than L_p approaches under strong input transformations (JPEG30, U512, D224, and MED5) because the small, indistinguishable perturbations are fragile to large pixel transformations. Specifically, our ACE achieves the best results against image scaling, and also performs effectively against other strong transformations. $cAdv^+$ yields the best performance in some cases, but at the cost of worse image quality (see Fig. 3). In addition, we can observe that, as expected, all the color transformation approaches are much more vulnerable to gray scale conversion than indistinguishable approaches. It is not surprising that the numbers for strong transformations are usually larger than those for mild ones, since stronger transformations inherently have larger impact on the original model prediction, as shown by the first row.

4.2.2 Adversarial Training

We explore the usefulness of adversarial training against ACE in the CIFAR-10 object recognition task [81]. The CIFAR-10 consists of 60000 32×32 color images in 10 classes. The official training split has 50000 images and the test split has 10000 images. In our experiments, we use the whole training split for training, and the first 500 testing images for model selection, and the rest 9500 for evaluating the model performance. We adopt the WideResNet-34-based undefended and L_∞ -robust models from [12], where the L_∞ -robust model is trained on 7-iteration PGD with $\alpha=2$ and $\epsilon = 8$. For ACE, we use its general formulation, ACE-PGD, with 50 iterations and $\alpha = 0.1$, and moderate parameters ($K = 64$, and $\epsilon = 8$) of the filter. More training details can be found in Appendix. Adversarial examples generated with this hyperparameter setting are shown in Fig. 9. These two adversarially trained models are denoted as AT-PGD and AT-ACE.

As can be seen from Table 7, adversarial training substantially improves model robustness in the case of both PGD and ACE, but with a trade off in the performance on

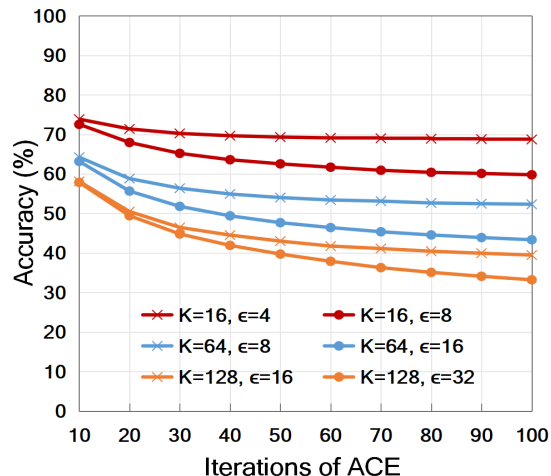


Fig. 10: Accuracy of AT-ACE (trained on ACE-PGD₆₄⁸) tested against ACE-PGD with varied hyperparameters.

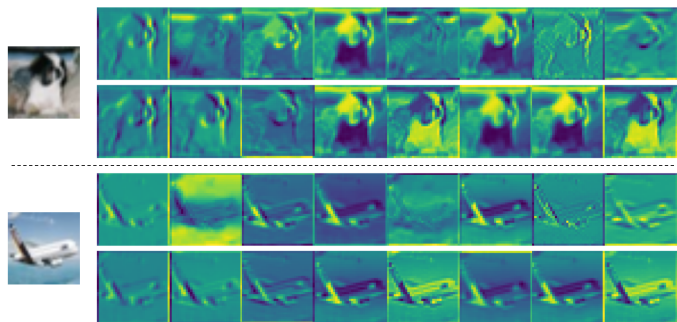


Fig. 11: Feature map visualization of the first convolutional layer. For each example, the top shows the original model and the bottom shows AT-ACE. AT-ACE yields smoother, more semantics-aligned image representations.

the original images. Further, the model adversarially trained on PGD is insufficient against ACE and vice versa. This result suggests that achieving comprehensive model robustness should consider different types of attacks. Fig. 10 shows how AT-ACE trained on a specific parameter setting of ACE, here ACE-PGD₆₄⁸, defends against ACE with different K and ϵ , and iterations. We can observe that AT-ACE trained on ACE-PGD₆₄⁸ can better cover the case of less aggressive settings with lower K and ϵ , while becoming less effective against more aggressive settings. In all cases, the robustness of AT-ACE is far higher than the result of the model without adversarial training, 7.14%.

We visualize the feature maps of the first convolutional layer for the original and the AT-ACE models in Fig. 11. As can be seen, the AT-ACE learns smoother, more semantics-aligned image representations than the original model, which is known to rely more on textures [82]. The effect may be due to the smoothing effects of the uniform color transformation applied to the training images.

5 CONCLUSION

We have proposed Adversarial Color Enhancement (ACE), which generates non-suspicious adversarial images by optimizing a color transformation within a principled paramet-

ric filter space. ACE can be controlled by directly imposing adjustable bounds on the filter parameters. Another advantage of our ACE is its simplicity and human-interpretable formulation. ACE advances the state of the art with respect to existing color transformation approaches, which are not guided by a principled action space and offer no means of explicitly controlling the color transformation. We have carried out a systematic robustness analysis of ACE, which is made possible by its principled action space.

Extensive experiments from the attack perspective have demonstrated the vulnerability of image classifiers, and also segmentation and aesthetic quality assessment algorithms, to our ACE. More experiments from the defense perspective validate the stability of ACE against strong input transformations, and also show that adversarial training can be used for improving model robustness against ACE. Cross-adversary analysis demonstrates that the conventionally studied L_p model robustness may not cover the robustness against ACE, implying that future research needs to consider different attacks for achieving more comprehensive model robustness.

We expect the robustness against ACE, and also the general color transformation will be further improved based on what we explored in this work. In addition to the adversarial robustness, another interesting direction is to explore the ACE-based adversarial training for improving model robustness against naturally occurring color shifts in common image processing practices.

ACKNOWLEDGMENTS

This work was carried out on the Dutch national e-infrastructure with the support of SURF Cooperative.

REFERENCES

- [1] C. Szegedy, W. Zaremba, I. Sutskever, J. Bruna, D. Erhan, I. Goodfellow, and R. Fergus, "Intriguing properties of neural networks," in *ICLR*, 2014. 1, 3
- [2] N. Carlini and D. Wagner, "Towards evaluating the robustness of neural networks," in *IEEE S&P*, 2017. 1, 3, 5, 6, 9
- [3] I. Goodfellow, J. Shlens, and C. Szegedy, "Explaining and harnessing adversarial examples," in *ICLR*, 2015. 1, 3, 5, 6
- [4] S.-M. Moosavi-Dezfooli, A. Fawzi, and P. Frossard, "DeepFool: a simple and accurate method to fool deep neural networks," in *CVPR*, 2016. 1
- [5] N. Papernot, P. McDaniel, S. Jha, M. Fredrikson, Z. B. Celik, and A. Swami, "The limitations of deep learning in adversarial settings," in *EuroS&P*, 2016. 1, 3
- [6] C. Xie, J. Wang, Z. Zhang, Y. Zhou, L. Xie, and A. Yuille, "Adversarial examples for semantic segmentation and object detection," in *ICCV*, 2017. 1, 7
- [7] Y. Zhao, H. Zhu, R. Liang, Q. Shen, S. Zhang, and K. Chen, "Seeing isn't believing: Towards more robust adversarial attack against real world object detectors," in *ACM CCS*, 2019. 1
- [8] A. Arnab, O. Miksik, and P. H. Torr, "On the robustness of semantic segmentation models to adversarial attacks," *IEEE TPAMI*, 2019. 1, 7, 8
- [9] Z. Liu, Z. Zhao, and M. Larson, "Who's afraid of adversarial queries? The impact of image modifications on content-based image retrieval," in *ICMR*, 2019. 1
- [10] G. Toliás, F. Radenovic, and O. Chum, "Targeted mismatch adversarial attack: Query with a flower to retrieve the tower," in *ICCV*, 2019. 1
- [11] A. Kurakin, I. Goodfellow, and S. Bengio, "Adversarial examples in the physical world," in *ICLR*, 2017. 1, 3, 4, 5, 6, 9
- [12] A. Madry, A. Makelov, L. Schmidt, D. Tsipras, and A. Vladu, "Towards deep learning models resistant to adversarial attacks," in *ICLR*, 2018. 1, 3, 4, 10, 18
- [13] J. Rony, L. G. Hafemann, L. S. Oliveira, I. B. Ayed, R. Sabourin, and E. Granger, "Decoupling direction and norm for efficient gradient-based l_2 adversarial attacks and defenses," in *CVPR*, 2019. 1, 3, 5
- [14] P.-Y. Chen, Y. Sharma, H. Zhang, J. Yi, and C.-J. Hsieh, "EAD: elastic-net attacks to deep neural networks via adversarial examples," in *AAAI*, 2018. 1, 3
- [15] J. Su, D. V. Vargas, and K. Sakurai, "One pixel attack for fooling deep neural networks," *IEEE TEVC*, vol. 23, no. 5, pp. 828–841, 2019. 1, 3
- [16] F. Croce and M. Hein, "Sparse and imperceptible adversarial attacks," in *ICCV*, 2019. 1, 3
- [17] B. Luo, Y. Liu, L. Wei, and Q. Xu, "Towards imperceptible and robust adversarial example attacks against neural networks," in *AAAI*, 2018. 1, 3
- [18] E. Wong, F. Schmidt, and Z. Kolter, "Wasserstein adversarial examples via projected sinkhorn iterations," in *ICML*, 2019. 1, 3
- [19] H. Zhang, Y. Avrithis, T. Furon, and L. Amsaleg, "Smooth adversarial examples," *EURASIP Journal on Information Security*, 2020. 1, 3
- [20] Z. Zhao, Z. Liu, and M. Larson, "Towards large yet imperceptible adversarial image perturbations with perceptual color distance," in *CVPR*, 2020. 1, 3
- [21] C. Xiao, J.-Y. Zhu, B. Li, W. He, M. Liu, and D. Song, "Spatially transformed adversarial examples," in *ICLR*, 2018. 1, 3
- [22] R. Alaifari, G. S. Albeti, and T. Gauksson, "ADef: an iterative algorithm to construct adversarial deformations," in *ICLR*, 2019. 1, 3
- [23] J. Gilmer, R. P. Adams, I. Goodfellow, D. Andersen, and G. E. Dahl, "Motivating the rules of the game for adversarial example research," in *arXiv preprint*, 2018. 1
- [24] L. Engstrom, B. Tran, D. Tsipras, L. Schmidt, and A. Madry, "Exploring the landscape of spatial robustness," in *ICML*, 2019. 1, 3, 4
- [25] C. Kanbak, S.-M. Moosavi-Dezfooli, and P. Frossard, "Geometric robustness of deep networks: analysis and improvement," in *CVPR*, 2018. 1, 3
- [26] K. Eykholt, I. Evtimov, E. Fernandes, B. Li, A. Rahmati, C. Xiao, A. Prakash, T. Kohno, and D. Song, "Robust physical-world attacks on deep learning models," in *CVPR*, 2018. 1, 3
- [27] A. Joshi, A. Mukherjee, S. Sarkar, and C. Hegde, "Semantic adversarial attacks: Parametric transformations that fool deep classifiers," in *ICCV*, 2019. 1, 3
- [28] H. Qiu, C. Xiao, L. Yang, X. Yan, H. Lee, and B. Li, "Semanticadv: Generating adversarial examples via attribute-conditional image editing," in *ECCV*, 2020. 1, 3
- [29] A. Bhattad, M. J. Chong, K. Liang, B. Li, and D. A. Forsyth, "Unrestricted adversarial examples via semantic manipulation," in *ICLR*, 2020. 1, 3, 5, 6, 7, 9
- [30] H. Hosseini and R. Poovendran, "Semantic adversarial examples," in *CVPRW*, 2018. 1, 3, 4
- [31] C. Laidlaw and S. Feizi, "Functional adversarial attacks," in *NeurIPS*, 2019. 1, 3, 4, 5, 6, 7, 9
- [32] A. S. Shamsabadi, R. Sanchez-Matilla, and A. Cavallaro, "ColorFool: Semantic adversarial colorization," in *CVPR*, 2020. 1, 3, 4, 7, 9
- [33] Y. Hu, H. He, C. Xu, B. Wang, and S. Lin, "Exposure: A white-box photo post-processing framework," *ACM Transactions on Graphics*, vol. 37, no. 2, p. 26, 2018. 1, 4
- [34] Z. Zhao, Z. Liu, and M. Larson, "Adversarial color enhancement: Generating unrestricted adversarial images by optimizing a color filter," in *BMVC*, 2020. 2
- [35] A. Rozsa, E. M. Rudd, and T. E. Boult, "Adversarial diversity and hard positive generation," in *CVPRW*, 2016. 3
- [36] A. Azulay and Y. Weiss, "Why do deep convolutional networks generalize so poorly to small image transformations?" *JMLR*, vol. 20, no. 184, pp. 1–25, 2019. 3
- [37] R. Zhang, J.-Y. Zhu, P. Isola, X. Geng, A. S. Lin, T. Yu, and A. A. Efros, "Real-time user-guided image colorization with learned deep priors," *ACM TOG*, vol. 36, no. 4, p. 119, 2017. 3
- [38] K. Grosse, P. Manoharan, N. Papernot, M. Backes, and P. McDaniel, "On the (statistical) detection of adversarial examples," in *arXiv preprint*, 2017. 4
- [39] X. Ma, B. Li, Y. Wang, S. M. Erfani, S. Wijewickrema, G. Schoenebeck, D. Song, M. E. Houle, and J. Bailey, "Characteriz-

- ing adversarial subspaces using local intrinsic dimensionality," in *ICLR*, 2018. 4
- [40] J. H. Metzen, T. Genewein, V. Fischer, and B. Bischoff, "On detecting adversarial perturbations," in *ICLR*, 2017. 4
- [41] C. Guo, M. Rana, M. Cisse, and L. van der Maaten, "Countering adversarial images using input transformations," in *ICLR*, 2018. 4, 9
- [42] A. Prakash, N. Moran, S. Garber, A. DiLillo, and J. Storer, "Deflecting adversarial attacks with pixel deflection," in *CVPR*, 2018. 4, 9
- [43] C. Xie, J. Wang, Z. Zhang, Z. Ren, and A. Yuille, "Mitigating adversarial effects through randomization," in *ICLR*, 2018. 4, 9
- [44] W. Xu, D. Evans, and Y. Qi, "Feature squeezing: Detecting adversarial examples in deep neural networks," in *NDSS*, 2018. 4, 9
- [45] N. Carlini and D. Wagner, "Adversarial examples are not easily detected: Bypassing ten detection methods," in *AISec*, 2017. 4
- [46] A. Athalye, N. Carlini, and D. Wagner, "Obfuscated gradients give a false sense of security: Circumventing defenses to adversarial examples," in *ICML*, 2018. 4
- [47] F. Tramer, N. Carlini, W. Brendel, and A. Madry, "On adaptive attacks to adversarial example defenses," in *NeurIPS*, 2020. 4
- [48] H. Zhang, Y. Yu, J. Jiao, E. Xing, L. El Ghaoui, and M. Jordan, "Theoretically principled trade-off between robustness and accuracy," in *ICML*, 2019. 4
- [49] F. Tramèr, A. Kurakin, N. Papernot, I. Goodfellow, D. Boneh, and P. McDaniel, "Ensemble adversarial training: Attacks and defenses," in *ICLR*, 2018. 4
- [50] C. Xie, Y. Wu, L. v. d. Maaten, A. L. Yuille, and K. He, "Feature denoising for improving adversarial robustness," in *CVPR*, 2019. 4
- [51] C. Xie and A. Yuille, "Intriguing properties of adversarial training at scale," 2020. 4
- [52] A. Shafahi, M. Najibi, M. A. Ghiasi, Z. Xu, J. Dickerson, C. Studer, L. S. Davis, G. Taylor, and T. Goldstein, "Adversarial training for free!" in *NeurIPS*, 2019. 4
- [53] E. Wong, L. Rice, and J. Z. Kolter, "Fast is better than free: Revisiting adversarial training," in *ICLR*, 2020. 4
- [54] L. Rice, E. Wong, and J. Z. Kolter, "Overfitting in adversarially robust deep learning," in *arXiv preprint*, 2020. 4
- [55] D. Zhang, T. Zhang, Y. Lu, Z. Zhu, and B. Dong, "You only propagate once: Accelerating adversarial training via maximal principle," in *NeurIPS*, 2019. 4
- [56] M. Balunovic, M. Baader, G. Singh, T. Gehr, and M. Vechev, "Certifying geometric robustness of neural networks," in *NeurIPS*, 2019. 4
- [57] M. Gharbi, J. Chen, J. T. Barron, S. W. Hasinoff, and F. Durand, "Deep bilateral learning for real-time image enhancement," *ACM TOG*, vol. 36, no. 4, pp. 1–12, 2017. 4
- [58] P. Isola, J.-Y. Zhu, T. Zhou, and A. A. Efros, "Image-to-image translation with conditional adversarial networks," in *CVPR*, 2017. 4
- [59] J.-Y. Zhu, T. Park, P. Isola, and A. A. Efros, "Unpaired image-to-image translation using cycle-consistent adversarial networks," in *ICCV*, 2017. 4
- [60] Y. Deng, C. C. Loy, and X. Tang, "Aesthetic-driven image enhancement by adversarial learning," in *ACM MM*, 2018. 4
- [61] J. Choi, M. Larson, X. Li, K. Li, G. Friedland, and A. Hanjalic, "The geo-privacy bonus of popular photo enhancements," in *ICMR*, 2017. 5
- [62] Z. Wu, Z. Wu, B. Singh, and L. S. Davis, "Recognizing instagram filtered images with feature de-stylization," in *AAAI*, 2020. 5
- [63] D. P. Kingma and J. Ba, "Adam: A method for stochastic optimization," in *ICLR*, 2014. 5
- [64] A. Kurakin, I. Goodfellow, S. Bengio, Y. Dong, F. Liao, M. Liang, T. Pang, J. Zhu, X. Hu, C. Xie *et al.*, "Adversarial attacks and defenses competition," in *The NIPS'17 Competition: Building Intelligent Systems*, 2018. 5
- [65] A. Krizhevsky, I. Sutskever, and G. E. Hinton, "Imagenet classification with deep convolutional neural networks," in *NeurIPS*, 2012. 5
- [66] K. He, X. Zhang, S. Ren, and J. Sun, "Deep residual learning for image recognition," in *CVPR*, 2016. 5
- [67] K. Simonyan and A. Zisserman, "Very deep convolutional networks for large-scale image recognition," in *ICLR*, 2015. 5
- [68] G. Huang, Z. Liu, L. Van Der Maaten, and K. Q. Weinberger, "Densely connected convolutional networks," in *CVPR*, 2017. 5
- [69] C. Szegedy, V. Vanhoucke, S. Ioffe, J. Shlens, and Z. Wojna, "Rethinking the Inception architecture for computer vision," in *CVPR*, 2016. 5
- [70] M. Larson, Z. Liu, S. Brugman, and Z. Zhao, "Pixel privacy: Increasing image appeal while blocking automatic inference of sensitive scene information," in *MediaEval Multimedia Benchmark Workshop*, 2018. 7
- [71] C. Y. Li, A. S. Shamsabadi, R. Sanchez-Matilla, R. Mazzon, and A. Cavallaro, "Scene privacy protection," in *ICASSP*, 2019. 7
- [72] R. Sanchez-Matilla, C. Y. Li, A. S. Shamsabadi, R. Mazzon, and A. Cavallaro, "Exploiting vulnerabilities of deep neural networks for privacy protection," *IEEE TMM*, vol. 22, no. 7, pp. 1862–1873, 2020. 7
- [73] B. Zhou, A. Lapedriza, A. Khosla, A. Oliva, and A. Torralba, "Places: A 10 million image database for scene recognition," *IEEE TPAMI*, vol. 40, no. 6, pp. 1452–1464, 2017. 7
- [74] X. Cheng, J. Lu, J. Feng, B. Yuan, and J. Zhou, "Scene recognition with objectness," *Pattern Recognition*, vol. 74, pp. 474–487, 2018. 7
- [75] Z. Zhao and M. Larson, "From volcano to toypshop: Adaptive discriminative region discovery for scene recognition," in *ACM MM*, 2018. 7
- [76] M. Everingham, S. A. Eslami, L. Van Gool, C. K. Williams, J. Winn, and A. Zisserman, "The PASCAL visual object classes challenge: A retrospective," *IJCV*, vol. 111, no. 1, pp. 98–136, 2015. 7
- [77] L.-C. Chen, G. Papandreou, F. Schroff, and H. Adam, "Rethinking atrous convolution for semantic image segmentation," *arXiv preprint*, 2017. 7, 8
- [78] H. Zhao, J. Shi, X. Qi, X. Wang, and J. Jia, "Pyramid scene parsing network," in *CVPR*, 2017. 7, 8
- [79] N. Murray, L. Marchesotti, and F. Perronnin, "Ava: A large-scale database for aesthetic visual analysis," in *CVPR*, 2012. 8
- [80] H. Talebi and P. Milanfar, "Nima: Neural image assessment," *IEEE TIP*, vol. 27, no. 8, pp. 3998–4011, 2018. 8
- [81] A. Krizhevsky, "Learning multiple layers of features from tiny images," 2009. 10
- [82] R. Geirhos, P. Rubisch, C. Michaelis, M. Bethge, F. A. Wichmann, and W. Brendel, "Imagenet-trained cnns are biased towards texture; increasing shape bias improves accuracy and robustness," in *ICLR*, 2019. 10

Zhengyu Zhao received the M.Sc. degree from Tianjin University, China, in 2017. He is currently pursuing a Ph.D. in computer science at Radboud University, The Netherlands. His research interests include adversarial examples, scene understanding, and image forensics. He has published in premier international conferences on computer vision and multimedia, such as CVPR, BMVC, and ACM MM. He is a recipient of the Outstanding Reviewer Award of BMVC 2020.

Zhuoran Liu received the M.Sc. degree from Radboud University, The Netherlands, in 2018. He is currently pursuing a Ph.D. in computer science at Radboud University. His research interests include multimedia privacy and security, recommender systems, and information retrieval.

Martha Larson is Professor of Multimedia Information Technology at Radboud University, The Netherlands. She is also affiliated with the Multimedia Computing Group at Delft University of Technology, The Netherlands. Her research interests are multimedia, recommender systems, and speech and language technology. She puts focus on responsible data science, and, in particular, online privacy.

APPENDIX A
ADDITIONAL EXAMPLES IN DIFFERENT TASKS

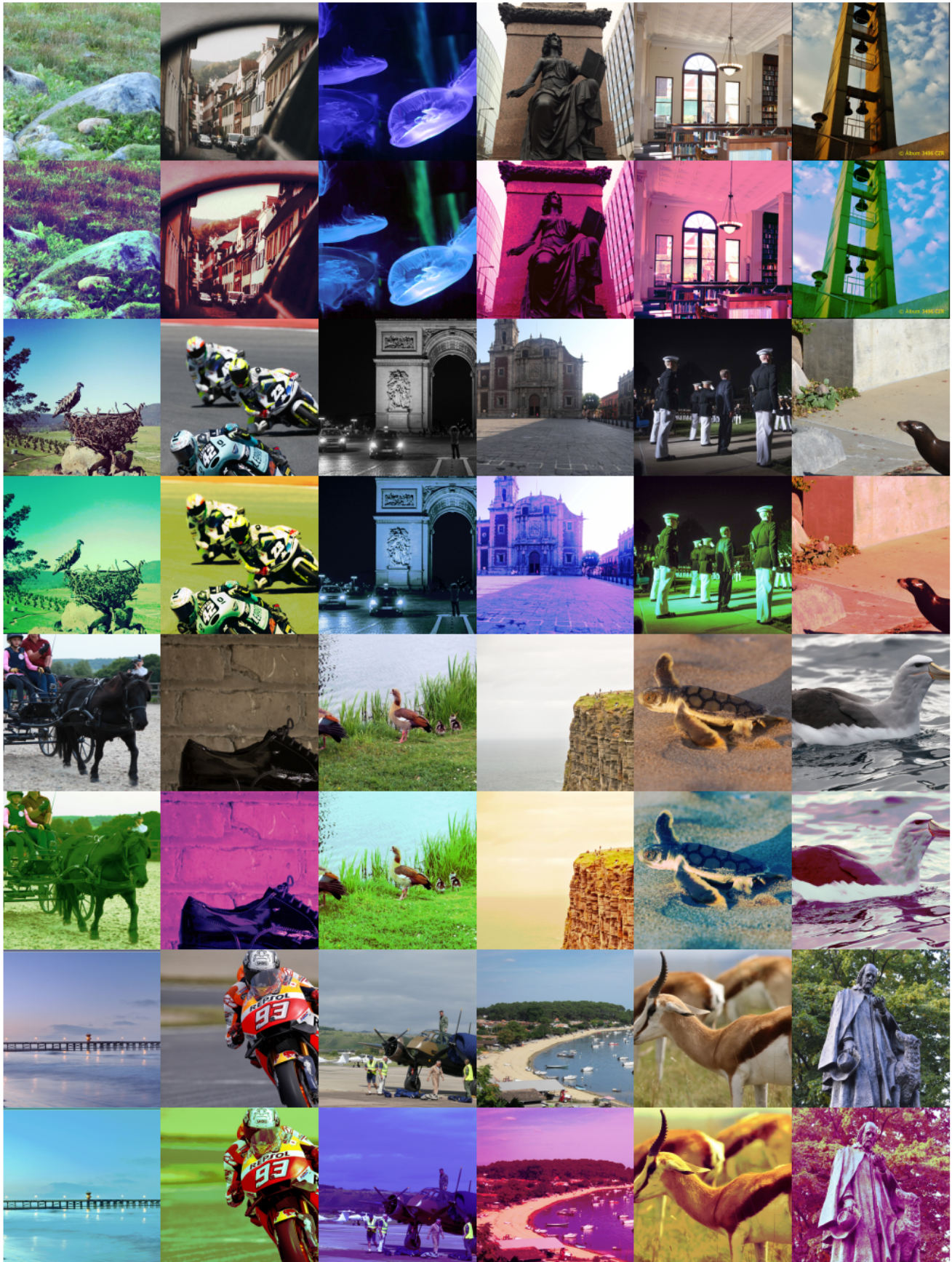


Fig. 12: Successful adversarial images on ImageNet (object recognition) with their original versions.



Fig. 13: Successful adversarial images on Places (scene recognition) with their original versions.



Fig. 14: Successful adversarial images on Pascal VOC (semantic segmentation) with their original versions.

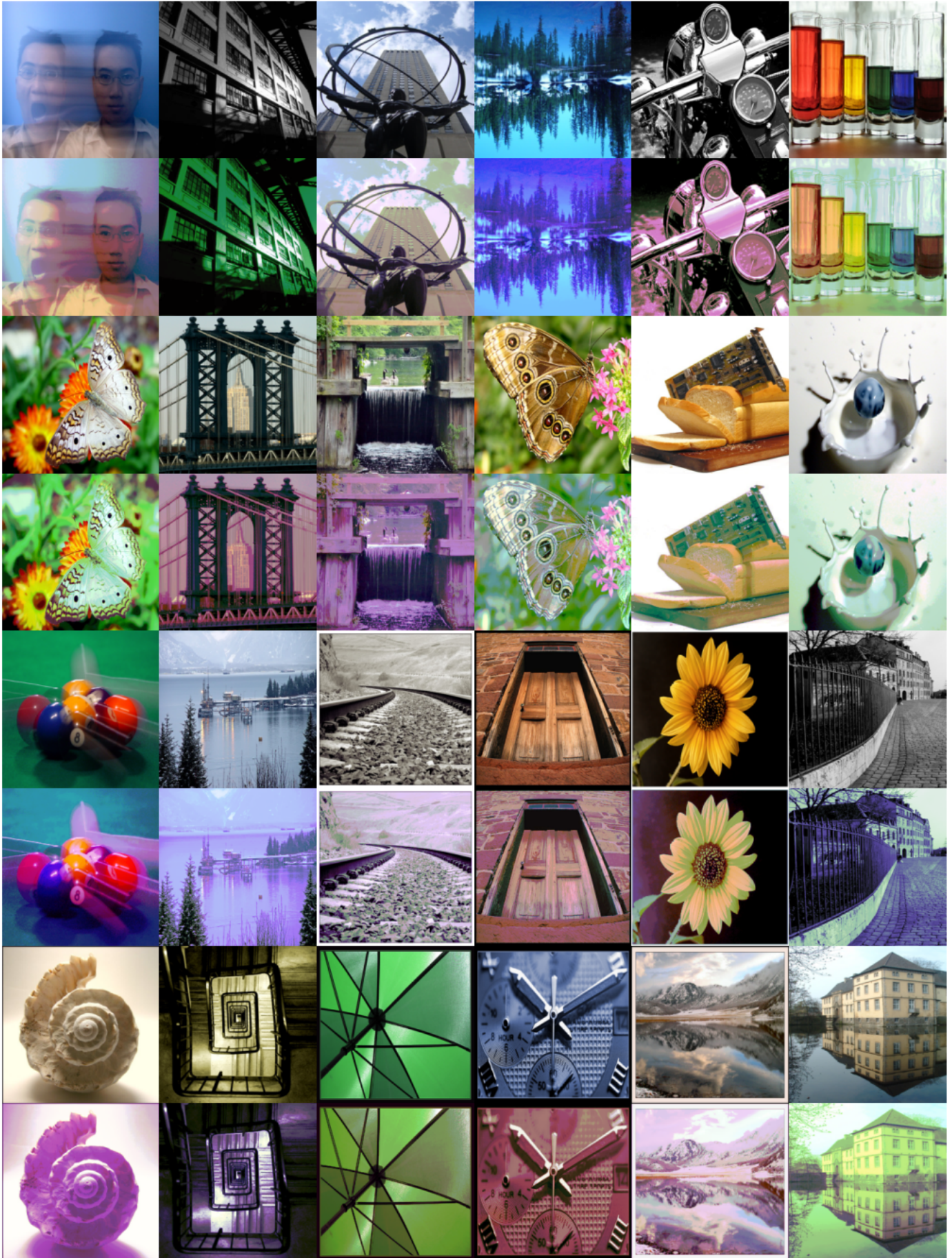


Fig. 15: Successful adversarial images on AVA (aesthetics prediction) with their original versions.



Fig. 16: Successful adversarial images achieved by ACE-Ins with color style guidance from Instagram filters.

APPENDIX B

DETAILS OF ADVERSARIAL TRAINING ON ACE

For the adversarial training on ACE, we use the same hyperparameter settings as in [12], and run 30 epochs of training. Details are summarized in Table 8 and the training curve is shown in Fig. 17. The model that achieves the best standard accuracy on the validation set is finally selected.

As can be observed in Fig. 18, fooling the adversarially trained model on ACE (AT-ACE) needs stronger transformations than the original model in general. In addition, fooling AT-ACE is much less successful (30.5% vs. 86.0%). Additional examples in Fig. 19 further confirm that our AT-ACE learns smoother and more semantics-aligned image representations than the original model.

TABLE 8: Adversarial training hyperparameters.

| | |
|------------------|----------|
| Batch_size | 128 |
| Number_of_epochs | 30 |
| Optimizer | SGD |
| Learning_rate | 0.1 |
| Momentum | 0.9 |
| Weight_decay | 2^{-4} |

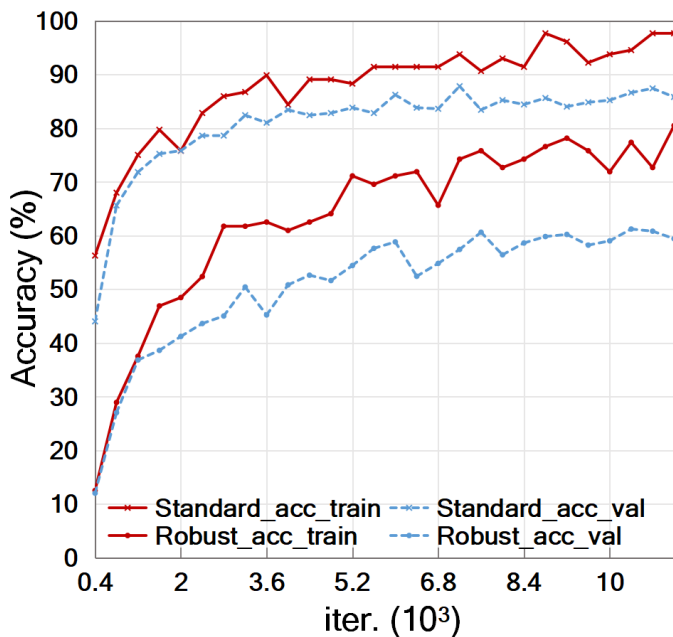


Fig. 17: The training curve of our ACE adversarial training.

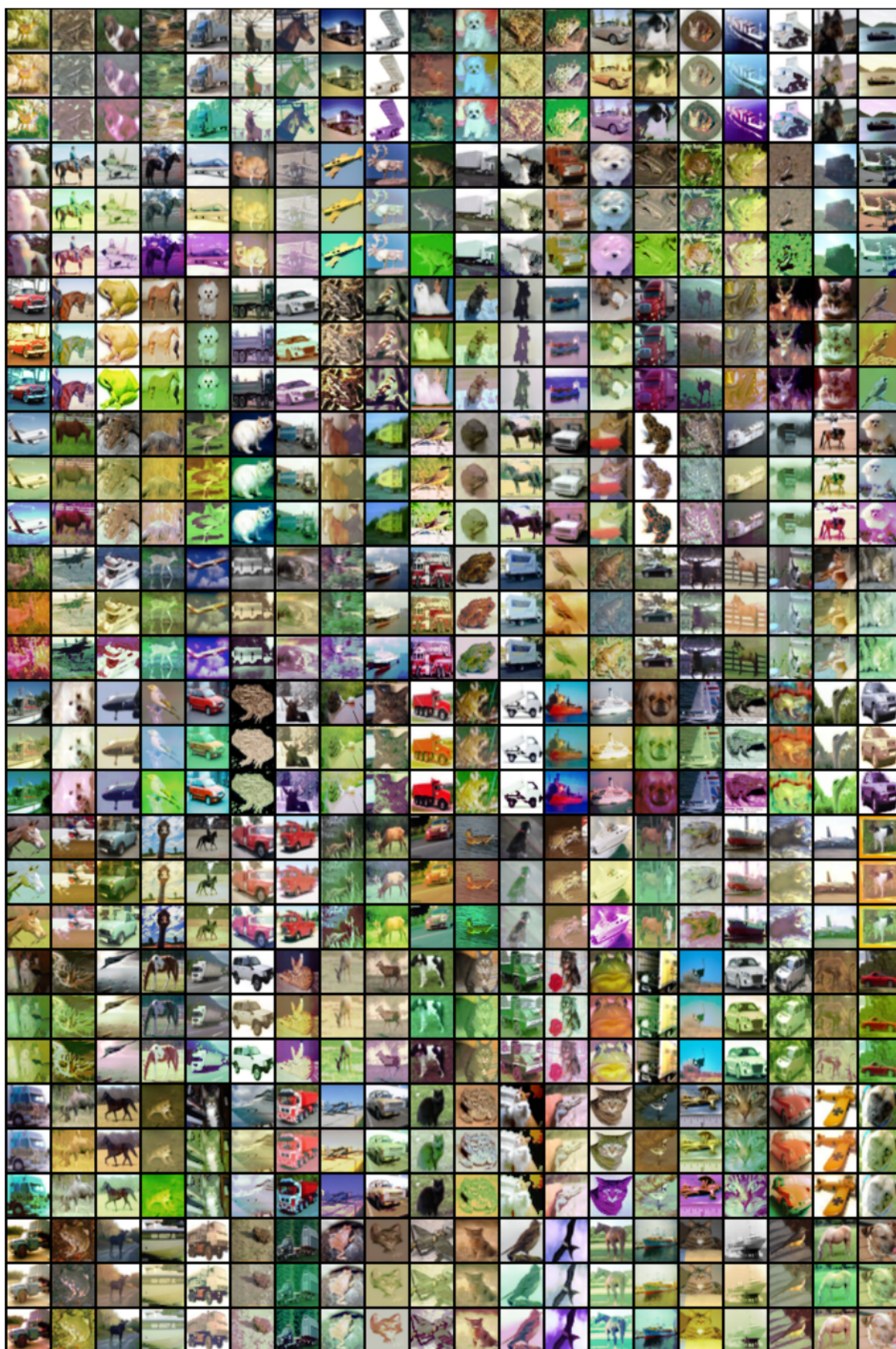


Fig. 18: Adversarial images on CIFAR-10 achieved by ACE against undefended (second row for each example) and ACE-robust (third row) model.

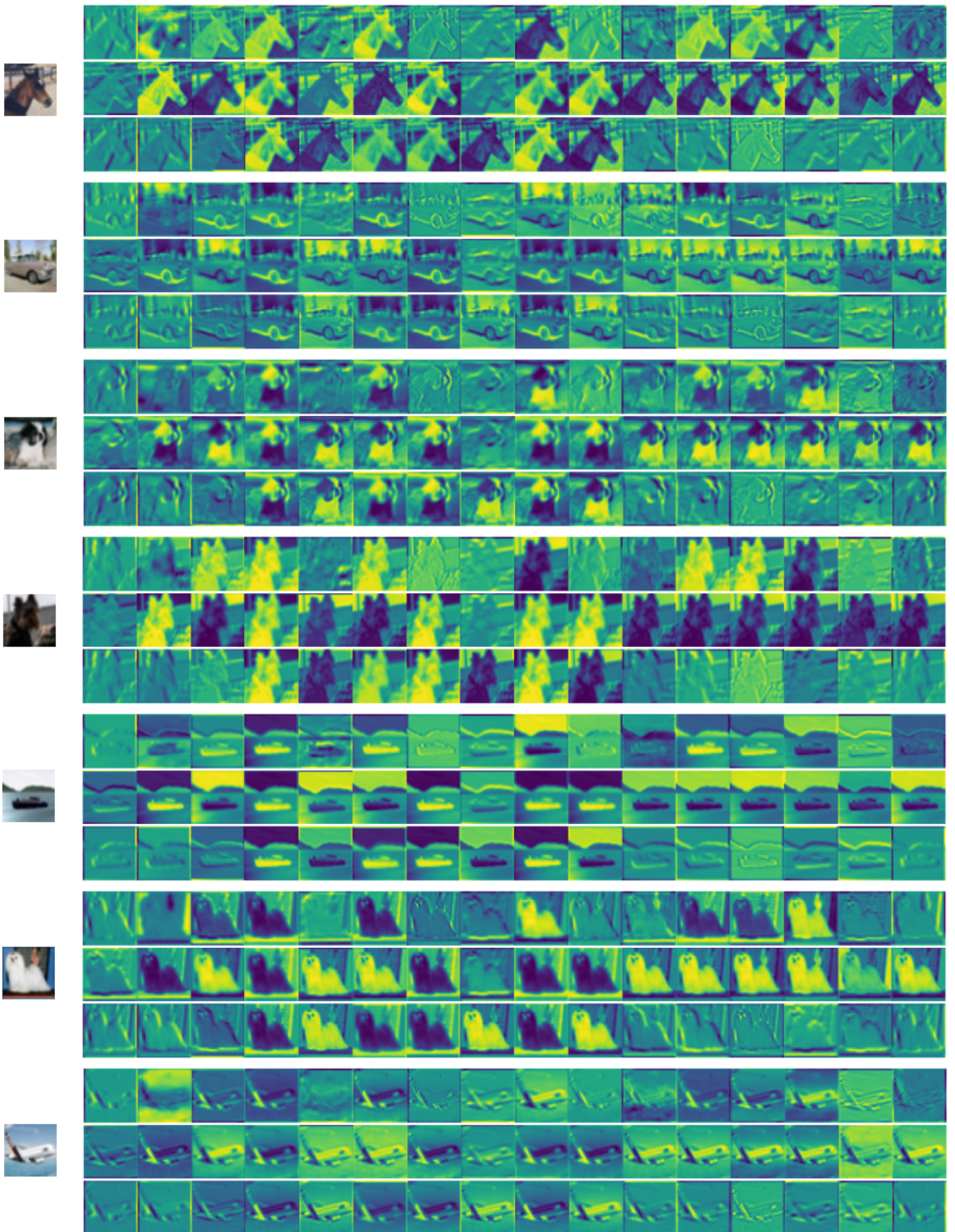


Fig. 19: Feature maps in the first convolutional layer of different models. For each example, from top to bottom, the undefended model, the PGD-robust model, and the ACE-robust model.